International Journal of Bioprinting

RESEARCH ARTICLE

Characterization and assessment of new fibrillar collagen inks and bioinks for 3D printing and bioprinting

Fatima Garcia-Villen[1,2,3]*, Amaia Guembe[4], José M. Rey[4], Teresa Zúñiga[4], Sandra Ruiz-Alonso[1,2,3], Laura Saenz-del-Burgo[1,2,3], Jesús M. Izco[4], José I. Recalde[4], Jose Luis Pedraz[1,2,3]*

[1]NanoBioCel Group, School of Pharmacy, University of the Basque Country (UPV/EHU), 01006, Vitoria-Gasteiz, Spain

[2]Biomedical Research Networking Center in Bioengineering, Biomaterials and Nanomedicine (CIBER-BBN), 01006, Vitoria-Gasteiz, Spain

[3]Bioaraba, NanoBioCel Research Group, 01009, Vitoria-Gasteiz, Spain

[4]Viscofan S.A., 31192, Tajonar, Spain

Abstract

Collagen is a cornerstone protein for tissue engineering and 3D bioprinting due to its outstanding biocompatibility, low immunogenicity, and natural abundance in human tissues. Nonetheless, it still poses some important challenges, such as complicated and limited extraction processes, usually accompanied by batch-to-batch reproducibility and influence of factors, such as temperature, pH, and ionic strength. In this work, we evaluated the suitability and performance of new, fibrillar type I collagen as standardized and reproducible collagen source for 3D printing and bioprinting. The acidic, native fibrous collagen formulation (5% w/w) performed remarkably during 3D printing, which was possible to print constructs of up to 27 layers without collapsing. On the other hand, the fibrous collagen mass has been modified to provide a fast, reliable, and easily neutralizable process. The neutralization with TRIS-HCl enabled the inclusion of cells without hindering printability. The cell-laden constructs were printed under mild conditions (50–80 kPa, pneumatic 3D printing), providing remarkable cellular viability (>90%) as well as a stable platform for cell growth and proliferation *in vitro*. Therefore, the native, type I collagen masses characterized in this work offer a reproducible and reliable source of collagen for 3D printing and bioprinting purposes.

Keywords: Type I collagen; 3D printing; 3D bioprinting; Tissue engineering; Bioink

***Corresponding authors:**
Fatima Garcia-Villen
(fgarvillen@ehu.eus)
Jose Luis Pedraz
(joseluis.pedraz@ehu.eus)

Citation: Garcia-Villen F, Guembe A, Rey JM, *et al*., 2023, Characterization and assessment of new fibrillar collagen inks and bioinks for 3D printing and bioprinting. *Int J Bioprint*, 9(3): 712. https://doi.org/10.18063/ijb.712

Received: September 19, 2022
Accepted: November 29, 2022
Published Online: March 16, 2023

1. Introduction

1.1. 3D printing for Tissue Engineering

The evolution of medicine is somehow parallel to the evolution of engineering and technology. Their combination has given rise to remarkable advances and fields of study such as "tissue engineering," a concept that was first coined in the late 1980s.

Nowadays, tissue engineering (TE) can be defined as an interdisciplinary field aiming to provide new strategies to repair, restore, maintain, or improve damaged tissues and/or whole organs by applying engineering strategies to combine biological components (cells, growth factors), drugs, and natural and/or synthetic materials. The resultant scaffolds or constructs obtained by the combination of these ingredients are intended to be implanted in the human body to regenerate and/or replace the damaged tissue, thus reducing (or even avoiding) the necessity of transplants.

From its inception, TE has made use of different techniques and approaches to shape the three-dimensional (3D) scaffolds, among which electrospinning and 3D bioprinting can be mentioned. Before the adaptation of 3D printing to TE (3D bioprinting), the artificial tissues produced were limited to two-dimensional cell sheets, which hindered their final performance[1]. The potential and usefulness of 3D bioprinting for this field of study is undeniable, since it not only allows for the creation of cell-laden, 3D structures (controlled deposition of materials, giving rise to precise shapes and scaffold dimensions), but also offers remarkable versatility due to the great diversity of 3D printing techniques[2]. In fact, the reviews of Ng *et al.*[3] and Ashammakhi *et al.*[4], among others, gathered some of the most outstanding studies in this field. The 3D printing and bioprinting techniques can be classified according to the ISO/ASTM 52900[5] for additive manufacturing. When it comes to TE, the 3D printing technique must be as non-detrimental as possible both with the materials and with the cells present in most cases. Briefly, other variations of this technique include material extrusion (mechanical and pneumatic)[6,7], material jetting (inkjet, microvalve, laser-assisted, acoustic)[8,9] and vat polymerization (stereolithography, digital light processing, two-photon polymerization)[10,11]. Extrusion, stereolithography, laser-assisted, inkjet, and microvalve-based printers have been the most used for 3D bioprinting in the last two decades[3]. Extrusion are pressure-driving printing techniques, in which the ink is propelled through a nozzle either by mechanical (axial piston or screw-driven) or pneumatic forces (air flow). Extrusion 3D bioprinting is the most prevalent approach due to its fast fabrication speed, ease of use, and compatibility with a wide range of materials, such as collagen and cells.

The difference between 3D printing and 3D bioprinting lies not only in the final scope of the 3D construct produced but also in the composition of the so-called "ink"[4,12-15]. Briefly, the concept "bioink" is used when cells are present in the product to be printed. On the contrary, "biomaterial ink," "biomaterial," or just "ink" can be used to make the difference. To draw a line between these two concepts is important, since the presence of cells would determine the 3D bioprinting conditions and so, the feasibility and success of the engineered tissue. Considering that the final scope of TE is to artificially reproduce a certain tissue or organ, the formulation of bioinks and biomaterial inks is a crucial step, since they will determine the properties of the construct (mechanical, rheological), the cell environment and, ultimately, its performance and integration with the native tissue(s) after implantation. With these premises, the usefulness of natural, biocompatible materials is easily foreseeable. Just to mention a few of them, materials such as gelatin, alginate, collagen, hyaluronic acid, or de-cellularized extracellular matrix (dECM) have been proven suitable as ingredients of TE 3D scaffolds. Nonetheless, due to their origin and intrinsic properties, these materials usually pose issues mainly related to their mechanical performance, extraction, and reproducibility.

1.2. Collagen and 3D bioprinting

In 3D bioprinting, collagen is one of the most useful and promising ingredients since it is a natural, fully biocompatible material for TE, together with the fact that it is a ubiquitous protein in the ECM. It possesses high affinity for adherent cells due to the presence of peptide sequences recognized by cell receptors. Moreover, the biodegradability of type I collagen by metalloproteinases act as chemotactic for cells such as fibroblasts, which further improves tissue regeneration[16]. Nevertheless, it is an ingredient with important limitations, such as its extraction process and the lack of batch-to-batch reproducibility, the influence of the environmental conditions (e.g., temperature could modify collagen viscosity) during the 3D printing process, and the low mechanical properties *in vitro* of the printed scaffolds[17,18]. At least 29 different types of collagens have been reported, which are classified, according to their structure, into: striatum (fibrous), non-fibrous (network forming), microfibrillar (filamentous) and those which are associated with fibril[19]. Type I collagen (fibrous) is the most common, primarily in connective tissue, in tissues such as skin, tendons, and bones. It consists of three polypeptide chains, two of which are identical, which are called chain α1 (I) and α2 (I)[20,21].

Most of the collagen inks available in the market are based on soluble collagen (limpid collagen solution, with no fibers), which requires a fibrillogenesis process before, after, or during the printing process, thus complicating the procedure, and possibly hinders cell viability and reproducibility[3]. The collagen extraction methods are based on the solubility of this protein in neutral saline solutions, acid solutions, and acid solutions with added enzymes. The method of extraction selected together with the processing parameters used through it highly influence the length of the polypeptide chains and final

collagen properties (viscosity, solubility, water retention, etc.)[21]. Usually, after the extraction, the resultant collagen solution is acidic (pH 2–3) and its viscosity is much lower than for fibrillar collagen[22]. The extraction method also determines the post-processing steps. For instance, acid-soluble collagen will require fibrillogenesis induction to obtain a self-standing scaffold after printing: transformation of tropocollagen into collagen fibrils and, subsequently, collagen fibers by means of a neutralization process. This process implies additional optimization, thus being another step inducing batch-to-batch variability. For the particular case of 3D bioprinting and TE, the use of non-denatured collagen that keeps the fibrillar structure closer to the native structure present in the original tissues, would allow a much more direct and rapid use since it involves a simpler neutralization process without further crosslinking to keep a consolidated structure after printing.

The importance of the optimization of extraction, concentration, neutralization, and collagen printing conditions has been highlighted in a recently published study[3,23]. In fact, bioinks with excessive collagen concentration are known to typically compromise cell viability due to the harsher printing conditions needed (high pressures for pneumatic extrusion 3D bioprinting) and the density of the resultant bioink: too dense bioinks could jeopardize nutrients and oxygen diffusion within the resultant scaffold, thus hindering cell viability and/or proliferation. Attempts to print acid collagen followed by *in situ* neutralization/crosslinking have also been made, but printability issues, low cell viability, or improper crosslinking were reported[3]. Stepanovska *et al.* have demonstrated that the optimization of the neutralization process is one of the key factors to be able to work with highly concentrated collagen bioinks[23]. Additionally, due to the low mechanical properties of pure *in vitro* collagen, only few studies have reported the use of collagen as a pure substance without additives[24].

At this point, it is plainly clear that collagen is a cornerstone protein for 3D bioprinting and TE due to its good biocompatibility, low immunogenicity, and natural abundance in a wide variety of tissues, making it a versatile ingredient for TE. However, its exploitation as a biomaterial is still limited due to the aforementioned drawbacks. The existence of a natural, standardized, and reproducible collagen source would be particularly useful for the progress of TE as it would minimize the batch-to-batch variability, which usually entails the optimization of the concentration and neutralization process of each batch, together with the 3D printing conditions and cellular viability.

The present manuscript demonstrates the reproducibility, reliability, and differential characteristics of two native, non-soluble, fibrillar collagen inks. Each collagen formulation was specifically designed for different 3D printing scopes: one of them (ColA) is intended as a biomaterial ink (to be 3D printed and subsequently neutralized); the other one (ColN) is specifically designed to be easily neutralized before the 3D bioprinting process, thus enabling the encapsulation of cells within the mass and so, the creation of a collagen bioink. Both formulations have been evaluated for rheology, mechanical properties, and *in vitro* biocompatibility. The most adequate printing conditions depending on the type of ink and the concentration have also been defined. Moreover, different ColN bioinks were prepared and loaded with two different types of cells to prove the effective and rapid neutralization and the high suitability of the formulation for 3D bioprinting and TE scopes. These bioinks have shown high cellular biocompatibility and proliferation for 12 days *in vitro*.

2. Materials and methods

2.1. Materials

The Viscofan Fibercoll-FlexA® (ColA) and Fibercoll-FlexN® (ColN) inks (bovine, collagen type I, 5% w/w) produced by Viscofan S.A. (Spain) were the base collagens used in this study. Each ink was subjected to a different treatment in order to optimize their final performance. ColA ink is intended to be 3D printed under acidic conditions and subsequently neutralized; on the other hand, ColN is also an acid collagen ink, but in this case, it is possible to neutralize the mass prior to the 3D printing (and 3D bioprinting) process, a process that is not possible with ColA.

TRIS buffer, hydrochloric acid solution, and NaOH were obtained from Sigma-Aldrich. Dulbecco's Modified Eagle's medium (DMEM; ATCC, 30-2002), fetal bovine serum (FBS), fetal calf serum (FCS), penicillin/streptomycin and phosphate-buffered saline (PBS, 1×, pH 7.4) solutions were purchased from Fisher Scientific (Madrid, Spain). WST-1 cell proliferation assay kit was obtained from Roche (Germany), Cell Counting Kit-8 (CCK-8) was also provided by Sigma-Aldrich, while Live/Dead™ (Invitrogen™) assay was purchased from Life Technologies (Madrid, Spain).

2.2. Ink characterization

2.2.1. Acidic ink preparation

Different collagen concentrations were prepared from ColA ink (Viscofan S.A., Spain). The required amounts of ColA ink were mixed with water by means of Luer lock syringes. Both syringes were connected with a Luer female-to-female connector (Fisher, USA), and mixed for a total of 40 times. As an example, to prepare a 3% (w/w)

collagen bioink, 3 g of ColA was loaded in one syringe, and 2 g of water was loaded in another syringe, connected and homogenized.

2.2.2. Neutral ink preparation

Starting from ColN ink (Viscofan S.A., Spain) with 5% of collagen content, the mass was neutralized by adding TRIS-HCl (1.5 M, pH 7.4) in a 3:2 and 2:3 volume ratio, thus diluting the collagen concentration to 3% (w/w) and 2% (w/w), respectively. Tris(hydroxymethyl)aminomethane (VWR, UK) was dissolved to a concentration of 1.5 M by magnetic stirring. To perform the neutralization, the fibrillar collagen ink was introduced in a 10-mL syringe with Luer lock, and the necessary amount of TRIS-HCl in a different syringe, with eccentric Luer lip. The syringes were connected through a Luer female-to-female connector (Fisher, USA), and mixed 40 times.

2.2.3. Rheology measurements

The rheology measurements were performed with a Haake Mars 40 rheometer (Thermo Scientific) equipped with a plate–plate geometry (20 mm ∅) and stainless steel smooth surface, working with a 0.8 mm gap at 25°C in all experiments, unless otherwise stated.

To perform the rheological measurements of the ColA acidic ink, a 2-cm layer of collagen was prepared between two Teflon sheets to avoid moisture loss. After a stabilization of the mass of 30 minutes at 4°C, a sample of 20 mm of diameter was punched out and placed in the bottom plate of the rheometer. When the measuring gap was reached, the acidic bioink was equilibrated for 10 minutes between the plates. The neutral ink (ColN) was prepared following the "neutral ink preparation" protocol (see section 2.2.2), and it was extruded in the bottom plate just after the neutralization. Once again, the sample was equilibrated for 10 minutes between the plates prior to analysis.

Oscillatory strain amplitude sweep tests were obtained by subjecting the samples to 1 Pa to 15,000 Pa in a logarithmic ramp with 6 points per order of magnitude, working at constant frequency (1 Hz) at 25°C. The temperature sweep oscillatory tests (0.1% amplitude, 1 Hz) were performed from 4°C to 37°C at a heating rate of 1 K/min. Subsequently, the same sample was cooled from 37°C to 4°C working under the same conditions.

Finally, the flow curves were obtained by subjecting the sample from 0.01 to 1000 1/s of shear rate (0.166 1/s steps), obtaining 6 points per order of magnitude.

2.2.4. Scanning electron microscopy

The micro-architectural properties of ColN collagen gels (before and after neutralization) were analyzed through cryogenic scanning electron microscopy (SEM). This technique has been chosen in view of already reported studies stating that cryo-SEM enables better preservation of the collagen microarchitecture[25]. ColN collagen were observed in a table-top TM4000Plus SEM (Hitachi) equipped with a coolstage (Deben UK Ltd) for cryo-SEM analysis. Samples were prepared as follows: Acid collagen sample was diluted to 0.5% (w/w) in milliQ water. Regarding the neutral samples, acid collagen was first neutralized with TRIS-HCl (1.5M, pH 7.5–7.6) until 2% (w/w). Then, the sample was further diluted with milliQ water until reaching 0.5% (w/w) concentration. Cryo-SEM analysis was performed by positioning a sample of the aforementioned dilutions in a cryo-SEM sample holder and rapidly freezing it to -50°C once inside the microscope chamber. Secondary electron (SE) images were obtained at 5 kV and medium vacuum conditions.

2.3. 3D printing

The acidic ColA and the neutral ColN neutral inks were prepared at different concentrations and printed with the pneumatic extrusion-based bioprinter BioX (Cellink). Squared 20 × 20 mm digital design with a 20% gyroid infill and two layers height (Figure 1A) were printed at different collagen concentrations in an attempt to determine the optimal printing conditions of each formulation. All the scaffolds were printed at room temperature with a 20-G nozzle (inner diameter 0.61 mm, Cellink). The speed and the pressure were adjusted for each collagen formulation. Additionally, a 27-layer scaffold (L × W × H: 20 × 20 × 20 mm) was obtained with ColA working at 300 kPa and 5 mm/s.

2.4. Cell cultures

Mouse fibroblast cell line (L929) was used for the *in vitro* cytotoxicity assays. These cells were cultured in DMEM supplemented with 1% (v/v) of penicillin/streptomycin and 10% (v/v) of FCS.

Regarding the 3D bioprinting and the production of cell-laden collagen bioinks, two types of cells were used: L929 and pluripotent D1 mesenchymal stem cells (MSC-D1). MSC-D1 cells were also cultured in DMEM 30-2002 (Gibco, Thermo-Fisher Scientific) supplemented with 1% (v/v) of penicillin/streptomycin and 10% (v/v) of FBS. In all cases, Tissue Culture Flasks (Corning® Costar®) were used for the expansion and maintenance of both MSC-D1 and L929 cells. Culture conditions were controlled by a cell culture incubator set at 37°C, with 5% CO_2 and 95% relative humidity.

2.5. *In vitro* cytotoxicity

The biocompatibility profile of ColA and ColN ink was assessed by means of the WST-1 assay kit, based on the

Table 1. Bioink concentration, cell type, and bioink code

Final ColN concentration (% w/w)	Mixture ratios (mL)			Cell type	Bioink code
	ColN	TRIS-HCl	DMEM (w and w/ cells)		
2.0	2	1.5	1.5	MSC-D1	2MSC
				L929	2L929
				No cells	2CTR
3.0	3	1	1	MSC-D1	3MSC
				L929	3L929
				No cells	3CTR

In all cases, the cellular density was maintained at 2×10^5 cell/mL.

steps indicated in the ISO 10993-5 for direct and indirect cytotoxicity.

A collagen film of approximately 2 mm thickness was prepared from ColA, followed by NaOH neutralization (50 mM, 30 min). The resultant, neutral film was rinsed with PBS twice (15 minutes each) to eliminate any excess of NaOH. Afterward, the neutral ColA film was submerged in complete DMEM supplemented with 1% (v/v) of penicillin/streptomycin overnight. Rounded scaffolds with 1 cm^2 surface were cut from the neutral collagen film and deposited in a 48-well plate. With respect to the neutral formulation, ColN collagen ink was neutralized by following the same procedure explained elsewhere (TRIS-HCl, 1.5 M, pH 7.4). Afterwards, corresponding DMEM amount was mixed up to 40 times to ensure a correct homogenization.

In order to quantify cellular viability, cell proliferation reagent WST-1 (Merck, Germany) was employed. WST-1 is a water-soluble tetrazolium salt (pink) that is cytosolically reduced by dehydrogenases into a formazan dye (yellow/orange) with absorbance peak at 440 nm, whose value is directly proportional to the amount of living cells. For the direct assay, L929 fibroblasts were incubated with a density of 3.12×10^4 cells/cm^2 for 24 h until fully confluent. Subsequently, acid and neutral gelified collagen inks at 2% (w/w) and 3% (w/w) were introduced within the cell-seeded wells for 24 h, which were later removed, and the WST-1 solution (1:44 dilution) was added for 1 h at cell culture conditions. Analogously, for the indirect assay, non-laden collagen samples were introduced in empty wells and covered in DMEM for 24 h. The resulting exudate was transferred to individual wells seeded with L929 cells (3.12×10^4 cells/cm^2) and incubated for 24 h. Then, the medium was removed, and the WST-1 cytotoxicity assay was performed as indicated above. All samples were done in triplicates with Latex® 1 cm^2 square membranes used as negative, cytotoxic controls, whereas positive controls consist of L929 fibroblasts with standard DMEM. Optical density (O.D.) of WST-1 reagent was measured at 440 nm in a microplate reader (Epoch, BioTek). The results are expressed as percentage of cell viability with respect to the positive control (Equation I). OD_{440s} refers to the average O.D. value of the test sample, while OD_{440b} stands for the blank, empty well. The cytotoxicity of the sample is inversely proportional to the percentage of cellular viability.

$$\text{Cell viability } \% = \frac{100 \times OD_{440s}}{OD_{440b}} \quad \text{(I)}$$

The viability of L929 cells seeded on the surface of each collagen mass was confirmed with a Live/Dead™ Viability/Cytotoxicity Kit, based on calcein-AM (green, live cells) and ethidium homodimer-1 (red, dead cells). Cell-seeded scaffolds were treated according to manufacturer's instructions, and samples were imaged with an inverted fluorescence microscope (Nikon, AZ100). The split channel images were subsequently merged by ImageJ® software (Fiji). This experiment was carried out in duplicates for each time point.

2.6. 3D bioprinting and culture of cell-laden scaffolds

2.6.1. Bioink formulation

Six different collagen bioinks were prepared starting from ColN in an attempt to evaluate the performance of this formulation during 3D bioprinting (Table 1). The acid mass (5% w/w), sterile ColN at room temperature was mixed with TRIS-HCl buffer (1.5 M, pH 7.5–7.6, sterilized by filtration with 0.2-μm nitrocellulose filters) by passing both ingredients (see Table 1 for ratios) from one syringe to another (Luer slip and Luer lock syringes, B Braun™), connected though a Luer lock connector. A total of 40 passes is enough to guarantee total collagen neutralization and homogeneous mixture. Right after this, the corresponding amount of culture medium (see Table 1 for ratios, with or without MSC-D1 or L929 cells suspended) is mixed with the neutralized ColN (approximately 20–25 syringe passes). Both the buffer and the collagen neutralization process are performed extemporaneously right before 3D

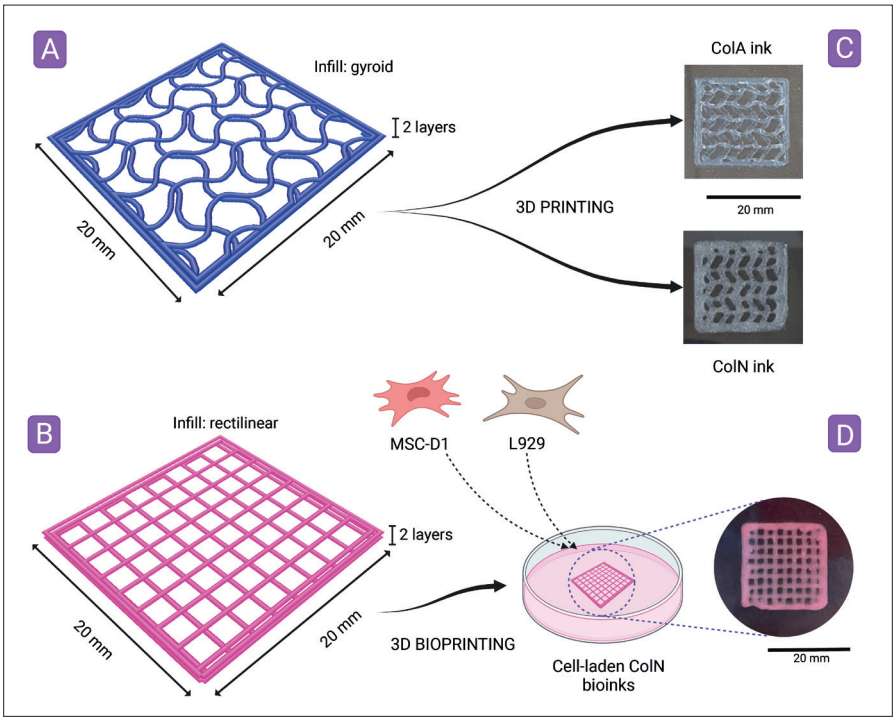

Figure 1. (A and B) CAD designs and dimensions for 3D printing and 3D bioprinting, respectively. (C and D) Real images of the resultant of collagen scaffolds after the 3D printing and 3D bioprinting. Once the printing conditions are adjusted, it is possible to obtain 3D scaffolds with adequate resolution with both ColA and ColN.

bioprinting. A cellular density of 2×10^5 cells/mL was used in all the bioinks.

2.6.2. 3D bioprinting and culture of cell-laden constructs

A square, CAD grid-like structure of 20 × 20 mm with a 20% rectilinear infill (two layers) (Figure 1B) was developed. The printing path was optimized through the G-code, and loaded into the 3D bioprinter BioX™, (Cellink) working on sterile conditions. The bioprinting process was performed with a 20-G nozzle (inner diameter 0.61 mm, Cellink) at a linear speed of 5 mm/s. The pneumatic extrusion of the bioinks was carried out between 50 kPa (for 2% collagen bioinks) and 70 kPa (for 3% collagen bioink), conditions which were defined in the previous 3D printing experiments. The concentrations were chosen in view of the 3D printing and rheology results. The temperature of the cartridge was maintained at 20°C by means of a temperature-controlled printhead (BioX, Cellink) to reproduce room temperature working conditions. The printing process was performed in sterile, polystyrene petri dishes (Φ 60 mm). Right after bioprinting, 3.5 mL of the corresponding culture medium (depending on the type of cells laden in each bioink) was added. The scaffolds were maintained at 37°C, in static conditions, inside a cell culture incubator (5% CO_2 and 95% relative humidity) for 12 days.

2.6.3. Cell viability and proliferation

The viability of the cells (MSC-D1 and L929) within the bioprinted scaffolds was determined by Live/Dead™ Viability/Cytotoxicity Kit (Invitrogen™). Cell-laden scaffolds were treated according to manufacturer's instructions and were observed and captured with an Eclipse TE2000-5 inverted fluorescence microscope (Nikon). Manual *z*-stacks were performed in all scaffolds (15 µm steps) for both calcein-AM and ethidium homodimer 1. The images were subsequently merged by using the microscopy software. This experiment was carried out in duplicates for each time point. The percentage of cellular viability (%) was determined by counting the amount of living and dead cells in each experiment and calculating the amount of living cells in the sample. A minimum of five replicates were used for the calculation of cellular viability.

Cell proliferation ability was determined using the Cell Counting Kit-8 (CCK-8) assay after 3D bioprinting. To do so, all the bioprinted scaffolds were incubated with 10% CCK-8 solution at 37°C for 24 h. At the end of each experiment, cellular proliferation was quantified by measuring the O.D. of the CCK-8 solution at 450 nm using a microplate reader (Tecan Infinite F200). These experiments were performed in sextuplicates and using three collagen non-laden scaffolds as controls. The results

are expressed as O.D. after subtracting the absorbance provided by the controls.

For each bioink, both the cell viability and proliferation were assessed at 0, 2, 4, 6, and 12 days after 3D bioprinting. To minimize the influence of cells growing over the petri dish (outside of the scaffold), the constructs were moved to new petri dishes before Live/Dead and CCK-8 experiments. All the scaffolds were maintained in static culture conditions (5% CO_2 and 95% relative humidity).

2.6.4. Mechanical properties of the bioprinted scaffolds

To study the influence of the bioprinting process, the culture conditions and the presence of cells within the constructs over the mechanical performance of the constructs, the textural properties were assessed at different time points. To do so, a 2% (w/w) and 3% (w/w) of ColN L929-laden bioinks were bioprinted, covered with culture medium and maintained at 37°C in a cell culture chamber for 24 h before the first compression measurement. Moreover, another batch of constructs were maintained *in vitro* for 12 days and subsequently subjected to uniaxial compression. The corresponding counterparts without cells were also printed and monitored as controls. Before the compression analysis, the culture medium was withdrawn and each scaffold was gently dried with tissue paper to eliminate excessive amount of liquid.

At this point, the 3D-bioprinted constructs were evaluated by means of uniaxial compression tests performed with a TA.XTplusC texture analyzer (Stable Micro Systems) equipped with a P/50 cylinder probe. The 3D constructs ($n = 6$) were compressed at 1 mm·seg^{-1} until 80% of strain. Compression data were collected and analyzed through Exponent Connect software. The compressive Young's moduli (Pa) values were obtained from the stress–strain curves, which were obtained during the uniaxial compression tests.

2.7. Statistical analysis

Statistical differences were determined by one-way analysis of variance (ANOVA, after confirming the normal distribution of the samples (Shaphiro–Wilk, $p > 0.05$, $n < 50$ in all cases). SPSS software was used to carry out the statistical analysis, and differences were considered significant at $p < 0.05$. Only significant differences are reported.

3. Results and discussion

3.1. Ink characterization

3.1.1. Rheology measurements

The oscillatory strain amplitude sweep allows to identify the linear viscoelasticity region (LVR), which defines the region when the viscoelastic parameters of the material are strain-independent below a critical strain. That is, the response of the material will only be dependent on its structure. The end of the LVR is sometimes difficult to define, since it does not correspond to the crossover point visible in the amplitude sweep test, but to a previous point in which the storage modulus (G′, also called "elastic modulus") and/or the loss modulus (G″, "plastic modulus") varies around 5% from the plateau value. From this point, the collagen bioink losses the elastic behavior and starts behaving like a viscous fluid. The oscillatory strain amplitude sweeps of ColA and ColN inks are shown in Figure 2A and **Figure S1**. It is clear that the end of the LVR depends on the collagen concentration, needing higher amplitude values to finish the LVR.

In fact, the higher is the collagen concentration (up to 5%), the wider is the LVR (Figure 2A and **Figure S1**). Likewise, the values of G′ and G″ within the LVR grow proportionally to the collagen content in the ink. This means that the ink is generally stiffer as the collagen concentration grows, disregarding the pH of the formulation (Figure 2A). Particularly, for the amplitude sweep profiles of the neutral inks, the modulus (G′ and G″) are significantly reduced in comparison with the acidic inks (pH 3), which can be explained by the amphoteric nature of the biopolymer. Rising the pH up to values closer to neutrality, the swelling capacity of the collagen is reduced, the protein reaches the lowest viscosity and maximum turbidity due to fiber aggregation[26]. This fiber aggregation is also driven by hydrophobic interactions and swelling reduction (water withdrawal). Since the collagen ink maintains the protein's native structure, the viscosity drops right after neutralization, and so do the elastic and viscous modulus. Despite these lower values, the mechanical properties of the printed scaffold are high and a self-standing structure is obtained without the need of jellification or further addition of crosslinkers.

The temperature sweep of the acidic and neutral collagen inks (Figure 2B) shows no elastic modulus variation (G′) from 4°C to 37°C and from 37°C to 4°C. The present results are contradictory to those previously reported by Li *et al.*, which found that type I collagen viscosity increased with increase in temperature[27]. A feasible explanation for this difference may be the sample concentration: Li *et al.* used highly diluted collagen solutions in acetic acid. In these conditions, collagen is soluble (molecular collagen, tropocolagen) and no collagen fibers are present (limpid dissolution). Under these circumstances, environmental changes such as temperature can trigger the fibrillogenesis, and so, the fiber formation and viscosity increase. The same results were reported for "Viscoll collagen bioinks"[28], working with porcine, soluble collagen type I; again,

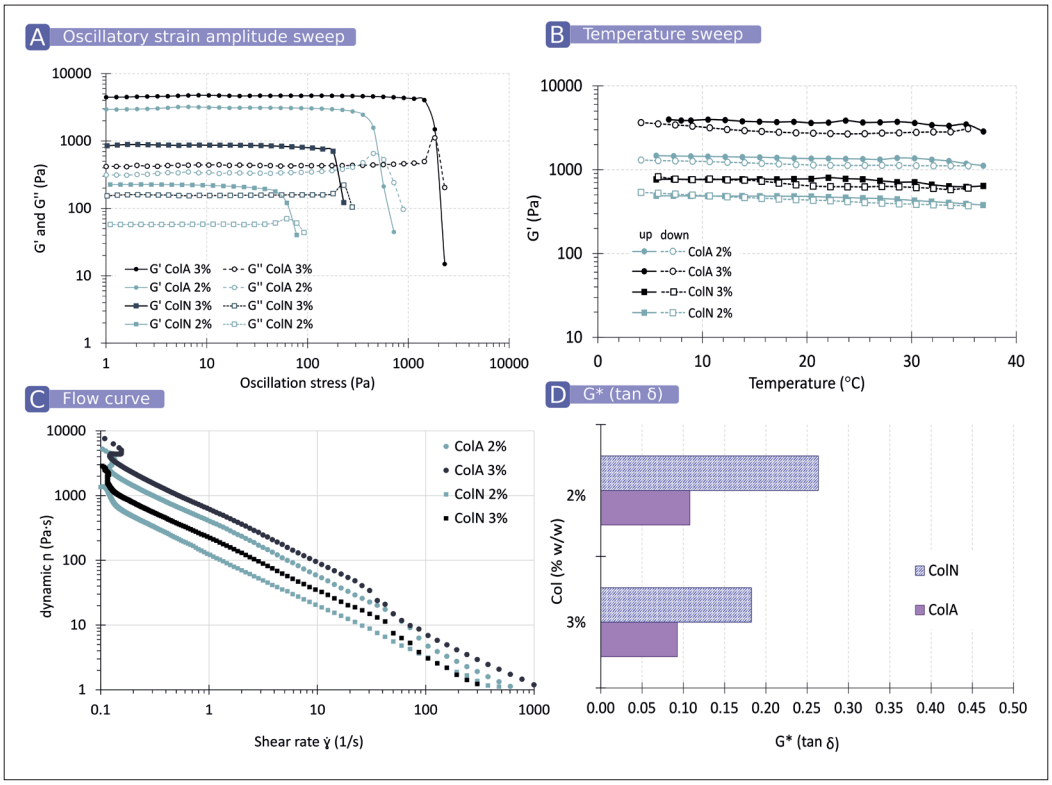

Figure 2. (A) Amplitude sweep and (B) temperature sweep of collagen inks at 2% (w/w) and 3% (w/w). (C) Flow curves of neutral and acid collagen inks at 2% (w/w) and 3% (w/w), showing dynamic viscosity. (D) G″ and G′ ratio (G*) of neutral and acid inks at 2% (w/w) and 3% (w/w).

fibrillonegesis and polymerization was triggered by factors like temperature. Collagen fibers are already present in both ColA and ColN, meaning that no fibrillogenesis occurs when the temperature changes. This is another advantage of ColA and ColN over soluble collagen bioinks, where temperature changes are known to trigger fibrillogenesis and so, changes in rheology. In view of the temperature sweep results, these inks can be printed at any temperature within this range without showing significant changes in their structural network, which is of great importance when working with 3D printing and bioprinting; it guarantees that environmental factors such as temperature will not influence the performance of the ink during the process. It is also worth to mention that the thermal stability between 32°C and 37°C demonstrates that these collagen inks could be printed under physiological conditions, which is desirable especially for cell-laden bioinks in TE.

For extrusion-based 3D printing and bioprinting, inks must meet certain requirements: they must be able to be liquid enough to allow their flow through the printing nozzle without jeopardizing cellular viability but solid enough to maintain their shape after printing and provide good printability. In terms of rheology, this implies that inks and bioinks with pseudoplastic behavior are desirable[13]. The decrease of the viscosity (Figure 2C) indicates that both ColA and ColN collagen inks have a shear-thinning, viscoelastic profile. Equivalent flow curve profile and apparent viscosity values have been previously reported for type I collagen solution[29,30]. This pseudoplastic profile of both ColA and ColN inks facilitates the printing process through pneumatic extrusion. Moreover, it is worth to mention that although both ColA and ColN show a parallel flow curve, the smaller viscosity values of ColN throughout the shear rate interval indicates that smaller forces are needed to induce ColN flow, thus implying friendlier printing conditions.

Inks with viscoelastic solid behavior (G′ > G″) tend to exhibit good printability and shape fidelity (Figure 2A)[31]. In fact, the larger is the difference between the storage modulus G′ and the loss modulus G″, the more adequate is the ink for direct extrusion bioprinting[24], which can be studied by using the tan δ or G* values (G″/G′). It has been reported that tan δ values between 0.2 and 0.5 are indicators of good printability and shape retention[32]. The closer is the loss tangent value to 0, the higher is the self-supporting ability and the higher is the stress needed to extrude an ink or bioink. Values closer to 0 are more prone to hinder cellular viability, while those closer to 1 ensure easy extrusion but exhibit poor shape retention and resolution. According to our results, it is clear that neutral

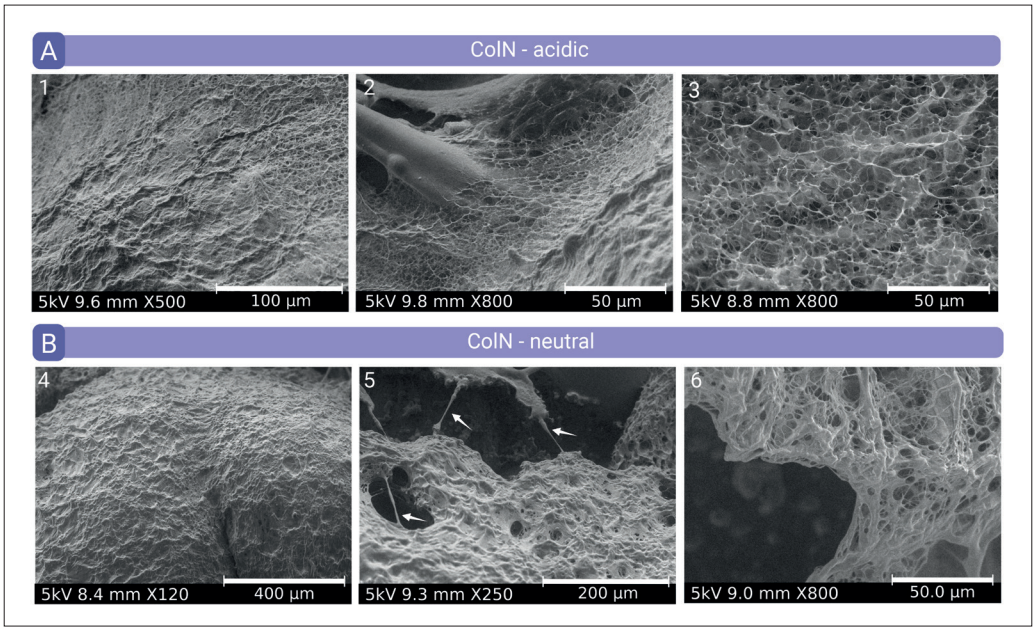

Figure 3. Cryo-SEM microphotographs of acid (A) and neutral (B) ColN samples at 0.5% (w/w). Samples were maintained at -50°C and the microscope was working at 5 kV under medium vacuum conditions. Insets 1 and 4 are images of the middle of the sample mass, showing the general texture of the sample; insets 2 and 5 are images taken at the borders of the samples. This region reveals significant differences between acid and neutral sample, since looser fibers with smaller diameter are visible in inset 2 in comparison with inset 5. Insets 3 and 6 are detailed images (800× magnification in both cases).

ColN (Figure 2D) shows tan δ values closer to those previously defined as "optimal"[32], particularly for the 2% (w/w) concentration. At this point, it is possible to state that ColN mass is more adequate for 3D bioprinting. Its influence on cell viability will be addressed in the following sections. Regarding ColA, the tan δ (G*) values were closer to 0 (including 4% [w/w] and 5% [w/w] concentrations [0.082 and 0.078, respectively, see **Figure S2**]), allowing us to predict that they will have better self-supporting ability but will need higher pneumatic pressure to be printed, which is confirmed in the following sections.

3.1.2. Scanning electron microscopy

SEM images of diluted acid and neutral ColN are shown in Figure 3. Clumping together of fibrils can be found in both acid and neutral inks, and images showing aspect similar to other collagen electron microscopy images have been shown in previous studies[25,33]. Nonetheless, larger void spaces are visible in acid collagen (Figure 3A), with the neutral counterpart being more compact. This compactness is related to the ability of collagen fibers to be closer to each other after the neutralization process, which is also related to the differential swelling capacity of collagen. Although it is impossible to determine their length due to their entanglement, it is evident that the fiber's diameter is higher after collagen neutralization (Figure 3B, arrows). It is well known that the disposition of collagen fibers depends on different environmental conditions like temperature, pH, and ionic strength. In fact, the closer are these environmental conditions to the physiological ones, the lower is the swelling capacity and the higher is the aggregation of collagen fibers. The neutralization process also creates an environment where collagen approaches its isoelectric point. In these conditions, this fibrous protein possesses neutral net charge, and this may also enable closer fiber interactions, thus promoting a more compact aspect, in agreement with the texture observed in Figure 3B. Moreover, the ionic strength of the environment and the salt type could also exert a significant influence on collagen microstructure and entanglement. It is known that high ion concentration leads to water withdrawal from collagen molecules, which promotes more collagen–collagen interactions (predominant hydrophobic interactions)[34].

Higher apparent viscosities have been reported for acidic ColA ink with respect to neutral ColN (Figure 2). That is, it is expected that more fiber interactions would lead to higher viscosities. Nonetheless, we observed the contrary. Inconsistences in rheological behavior of type I collagen have already been reported[27]. In the acidic ColA ink, fibrils are swollen up to its maximum capacity and are more freely and homogeneously distributed in the whole collagen ink, which enables them to actively participate in the formation of an internal network that exerts higher resistance to external stresses (higher viscosity). It can be hypothesized that the neutralization process changes the environment and induces some release of water from collagen fibrils, which may aggregate between each other. Under these

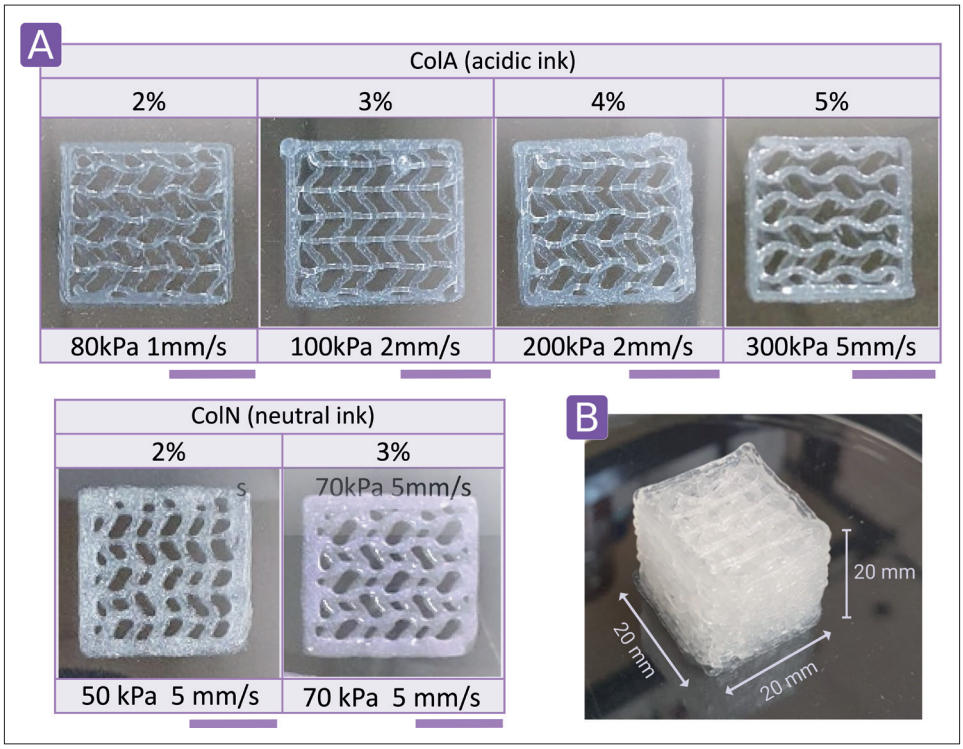

Figure 4. 3D-printed collagen scaffolds at different concentrations together with their printing conditions (pressure and speed) for each case. Scale bars: 10 mm. (B) Scaffold printed with ColA ink (acidic ink, 5% w/w) with 27 layers. As it can be seen, the consistency of this ink is appropriate to produce complex structures without collapsing.

conditions and despite their higher dimensions, the number of "free independent" fibers within the network reduces and, therefore, there is more "space" available between them and less cohesiveness. This can be translated into lesser interactions during stress application (rheology measurements) and therefore, lower viscosity values. Similar results were observed for viscosity values of type I collagen in the presence of salts, thus supporting the present hypothesis[27].

3.1.3. 3D printing

The resolution, shape fidelity, and cell viability are important factors determining the suitability of the resultant scaffold for TE. As previously mentioned, high-viscosity bioinks usually led to high-quality structures with remarkable shape fidelity, while lower viscosities are related to higher cell viability and softer structures, which are unable to maintain their shape after printing.

The ColA mass was bioprinted at different concentrations in order to obtain a continuous, self-standing scaffold with the maximum shape fidelity and resolution. The pressure and speed were adjusted to guarantee a continuous flow. Higher concentrations of collagen require higher printing pressures (Figure 4). The necessity of higher printing pressures for the acidic formulation with respect to the neutral ink (ColN) is in agreement with the rheology studies (Figure 2); the acidic inks have higher consistency compared to the neutral ones (see tan δ values). This great consistency allows for the printing of tall, complex scaffolds as shown in Figure 4B.

When it comes to cell-laden scaffolds produced by pneumatic extrusion 3D bioprinting, it is desirable to obtain the highest resolution and shape retention with the lowest pressure to guarantee cellular viability. In fact, a recent systematic review confirmed that cell viability is inversely proportional to printing pressure and directly proportional to printing nozzle diameter[35,36]. Bearing in mind that the nozzle used to obtain all the scaffolds was the same, the 3D printing performance of the neutral inks (Figure 4) is more desirable since they provide good resolution with low printing pressures together with an optimal pH for the cells to be laden.

3.1.4. In vitro cytotoxicity

None of the *in vitro* studies have revealed evidence of cell toxicity by acid or neutral collagen formulations toward L929 cells, as demonstrated by the cellular viability percentages provided by the WST-1 test, as presented in Figure 5A and B. In fact, the cellular viability was systematically equivalent or even superior to the positive control. Although no statistically significant differences

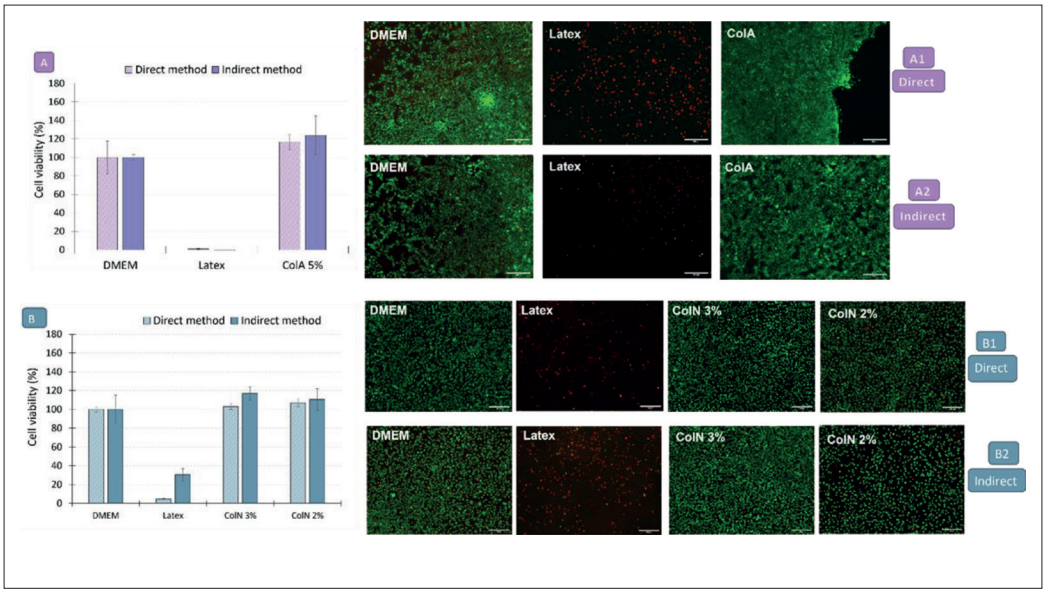

Figure 5. Cell viability (%) of L929 fibroblast seeded on ColA (A1 and A2) and ColN (B1 and B2) inks according to WST-1 (A, B) and Live/Dead assays (1–2). Scale bars: 200 μm.

have been detected, the fact that the cellular viability tend to be higher with respect to the control suggests that the collagen inks could induce or favor cellular growth.

Particularly for ColN, cytotoxicity results (Figure 5B) indicate that the concentration of TRIS-HCl used (1.5 M) is non-cytotoxic, thus indicating that the neutralization procedure can be used for the formulation of cell-laden bioinks. The final concentration of TRIS-HCl in the scaffold is approximately 250 mM, which is less than the concentration of other medical materials approved by the FDA and clinically available, like Tromethamine injection[37] which is used to prevent and treat severe metabolic acidosis. In addition, the concentration of collagen does not appear to be a parameter affecting cell viability. Therefore, any differences on cellular viability detected after the 3D bioprinting of neutral collagen bioinks would probably be related to the bioprinting conditions rather than to the collagen concentration. Regarding the ColA ink (acidic ink, 5% w/w), these tests confirm the full biocompatibility of the formulation (both indirect and direct) after simple neutralization (Figure 5A).

3.2. 3D bioprinting and culture of cell-laden scaffolds

3.2.1. Cell viability and proliferation

Right after the 3D bioprinting of ColN, cell-laden bioinks, dead cells (red) are by far outnumbered by living cells (green), as shown by the Live/Dead™ assay results presented in Figures 6 and 7. At this point, the majority of dead cells are located on the verge of the printing lines, revealing that the shear stress of the bioink extruded through the printing gauge induces cell death. Next to the printing nozzle's wall, the flow is faster and the shear stress is higher, which causes cell deformation and subsequent death[35]. Notwithstanding this fact, the bioprinting process herein reported can be considered harmless for L929 and MSC-D1 since (as shown by the cell viability results represented in Figure 8), 90% of cellular viability has been reported at day 0 in all cases. Moreover, living cells are homogenously distributed throughout all the printing lines, thus suggesting that the diffusion of nutrients and oxygen inside the bioink network is sufficient to guarantee cellular growth.

The cellular viability has been quantified based on this analysis with results shown in Figure 8. Nevertheless, the unreliability of the quantification methodology increases with time, since cells start to confluence and to become indistinguishable, as easily observable in some of the Live/Dead images at day 12 (Figure 7A, day 12). This fact must be taken into consideration during the interpretation of results, which means that the cellular viability reported for days 6 and 12 could be higher than estimated. Fibroblasts maintained a constant and high viability throughout the whole experiment (≥90%) (Figure 8A). No significant differences have been found between different collagen concentrations. This is in agreement with the direct and indirect cytotoxicity tests mentioned in section 3.1.4 (Figure 5) and even with some results in the literature from collagen bioinks within the same order of concentration[24,38]. It is also worth to mention that the collagen used by Osidak *et al.*[28] was a soluble collagen that required fibrillogenesis triggered by TRIS-HCl neutralization at 4°C and then collagen

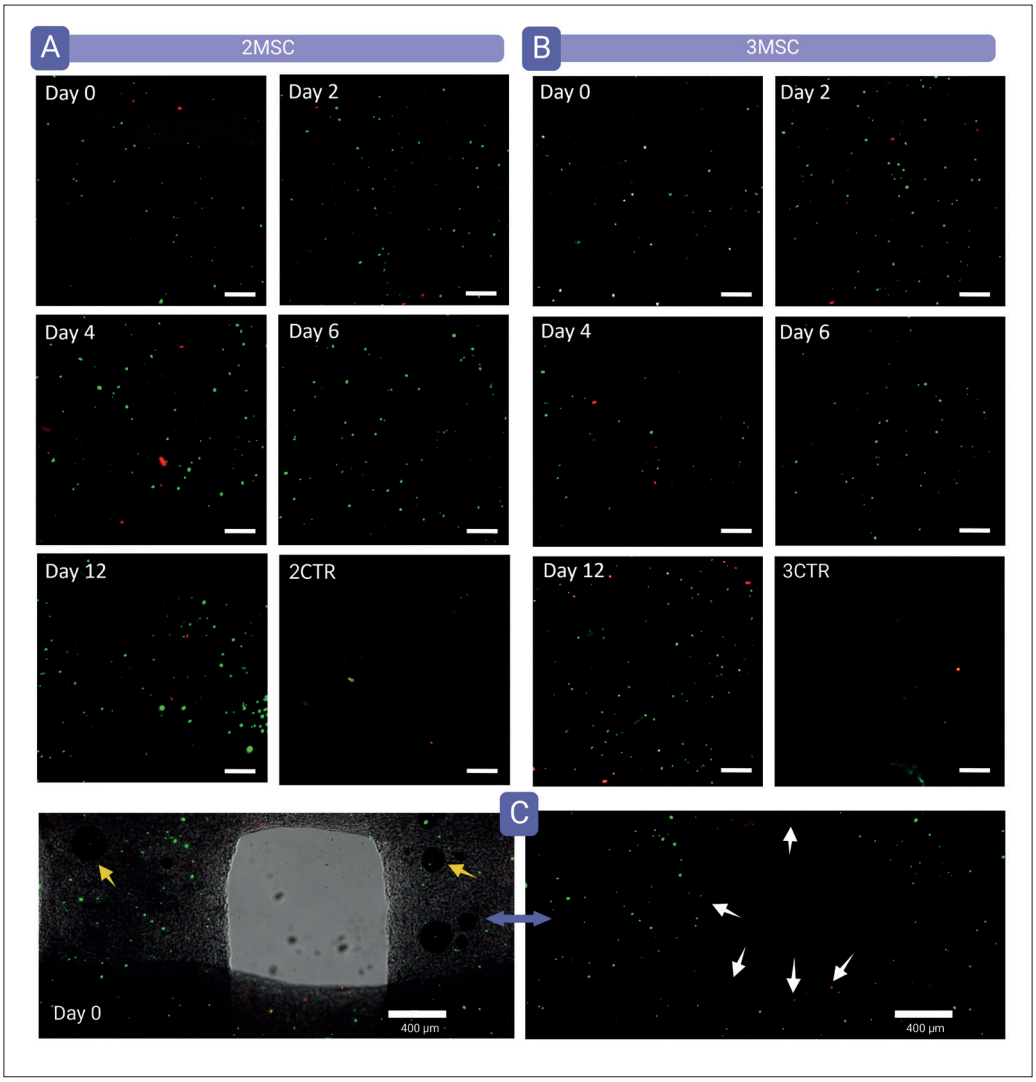

Figure 6. Fluorescence microscopy for the (A) 2MSC and (B) 3MSC scaffolds. Live cells (green) and dead cells (red) were stained with calcein-AM and ethidium homodimer-1, respectively. These microphotographs were obtained by performing z-stack of the scaffolds and merging both channels (4× magnification). (A and B) The scale bar corresponds to 200 µm. (C) Detailed image at day 0 of the 3D-printed scaffold merging brightfield, calcein-AM, and ethidium homodimer-1 channels. Yellow arrows (left) point to air bubbles in the bioink; white arrows (right) mark the location of dead cells in the printing line edge.

polymerization induced by the increase in temperature (at 37°C). In other words, these authors were able to extrude type I collagen with good cell viability results, but the 3D bioprinting process was more complex, needing a careful control of factors like temperature throughout the entire process.

The metabolic activity of MSC-D1 and L929 determined by CCK-8 is shown in Figure 9. CCK-8 contains WST-8 (a water-soluble tetrazolium salt, yellow) that can be reduced by dehydrogenase in the cell to a corresponding formazan dye (yellow/orange) that absorbs at 450 nm. The absorbance of the formazan salt is proportional to the number of living cells.

The absorbance values (O.D.) generated by the CCK-8 tests are rather low when compared to the results usually obtained in 2D cultures. This fact can be explained by the low cellular density within the bioinks (2×10^5 cell/mL) and the 3D nature of the scaffolds. In these conditions, the WST-8 must reach the cells embedded within the 3D scaffold and be metabolized, and the resultant formazan dye must be released to the culture medium to be effectively quantified. In 2D cultures, the CCK-8 test takes about 4 h to complete. Nonetheless, it has been observed that 4 h are not enough to achieve reliable and reproducible O.D. data from the 3D collagen scaffolds. Instead, the CCK-8 assay was left in contact with the scaffolds for 24 h.

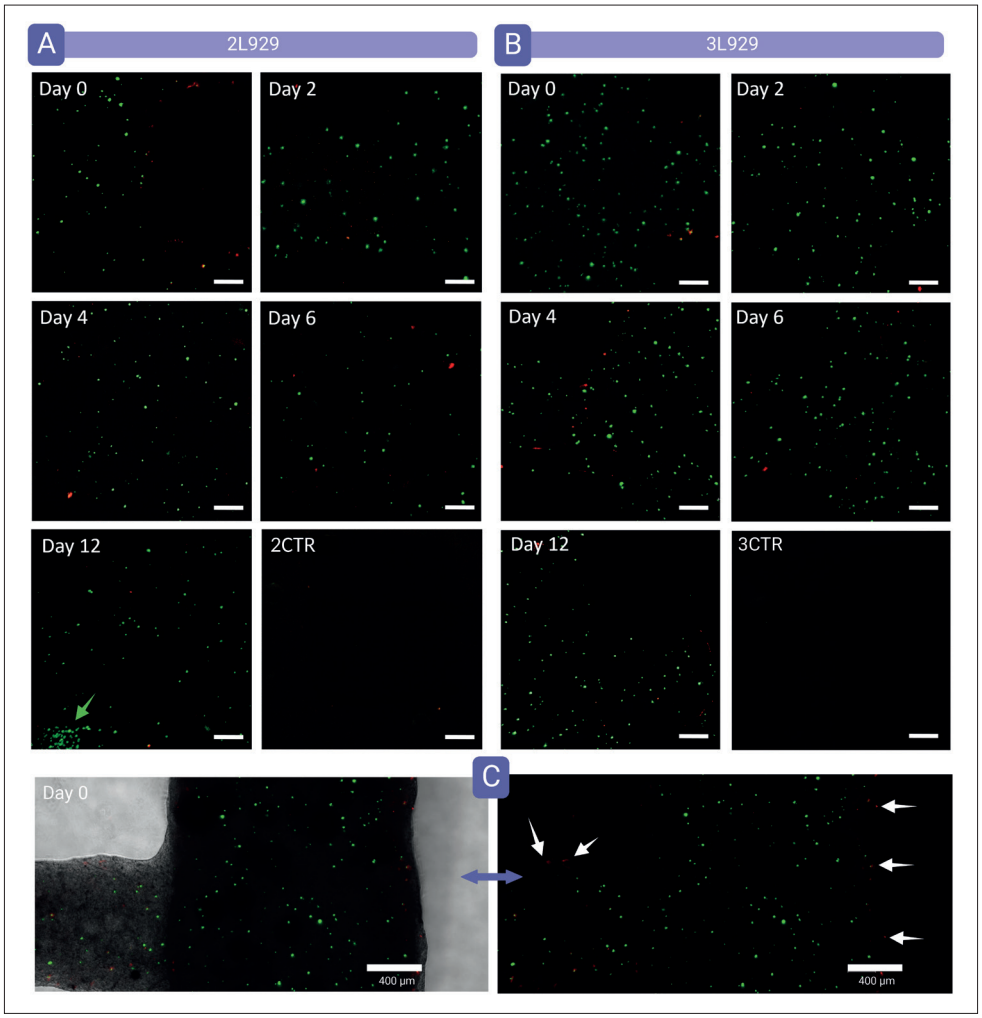

Figure 7. Fluorescence microscopy for the 2L929 and 3L929 scaffolds. Live cells (green) and dead cells (red) were stained with calcein-AM and ethidium homodimer-1, respectively. These microphotographs were obtained by performing z-stack of the scaffolds and merging both channels (4× magnification). (A and B) The scale bar corresponds to 200 µm. The green arrow at day 12 marks a zone of confluent cells. (C) Detailed image at day 0 of the 3D-printed scaffold merging brightfield, calcein-AM, and ethidium homodimer-1 channels. White arrows (right) mark the exact location of dead cells in the printing line edge.

No absorbance was detected from the scaffolds at day 0 (Figure 9), which means that cells were not metabolically active right after the printing process, probably due to the stress to which they have been subjected throughout the bioink formulation (trypsinization, centrifugation, counting) and the bioprinting process itself. Nevertheless, the Live/Dead™ assay demonstrated that most cells were alive (green cells) just a few h after the bioprinting process (Figures 6 and 7).

The metabolic activity of cell increased with time, demonstrating continuous cell proliferation. The O.D. values of 2L929 and 3L929 scaffolds at 12 days were significantly higher than the rest of the data. This can be explained by the proliferation of cells over the petri dish, outside of the scaffold (Figure 9). Despite introducing a distortion to the CCK-8 test results, this fact clearly demonstrates that cells were able not only to proliferate but also to migrate within the scaffold.

3.2.2. Mechanical properties

The uniaxial compression analysis of all the bioprinted scaffolds revealed that they were able to resist 80% strain without permanent deformation (e.g., fractures), as demonstrated by the absence of peak forces between 0% and 80% of strain (Figure 10A). The shape of these curves are in agreement with those already reported by Osidak *et al.*, who worked with 3D-printed collagen scaffolds from soluble porcine origin collagen type I[28]. On the other hand, the mechanical values of their scaffolds have a higher order or magnitude than those reported here. These differences can be ascribed to the differential shape

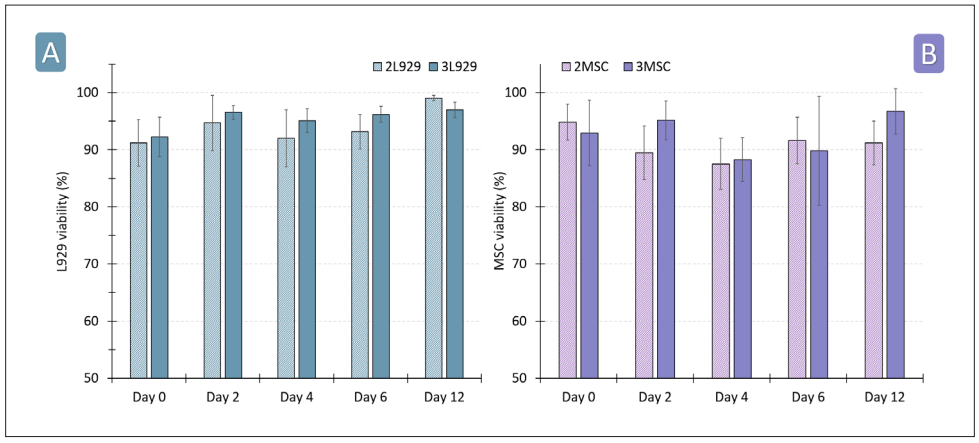

Figure 8. Cell viability (%) of fibroblasts (A) and mesenchymal cells (B) cultured within the bioprinted scaffolds. Results are based on Live/Dead™ assay.

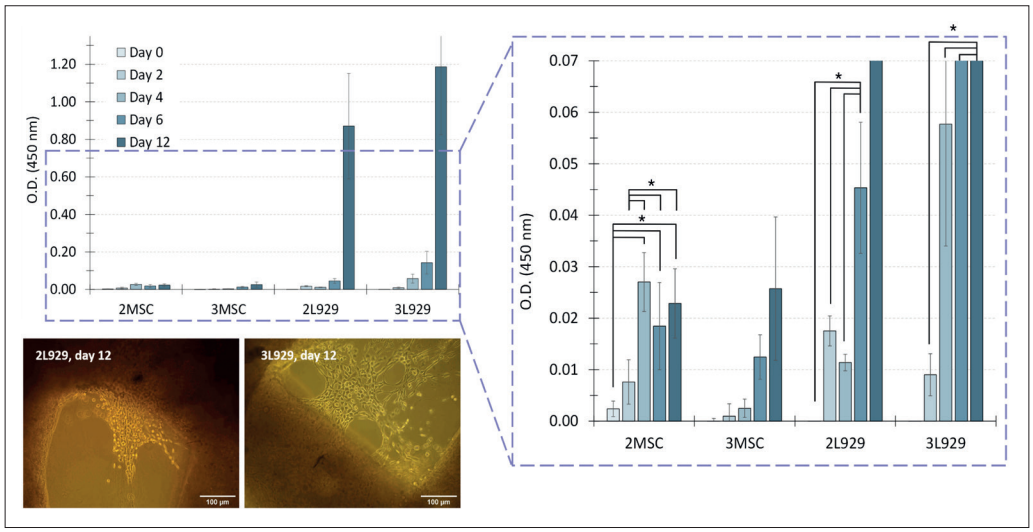

Figure 9. Optical density (O.D.) obtained after culturing the cell-laden scaffolds (2MSC, 2L929, 3MSC, 3L929) in 10% of CCK-8 for 24 h (mean ± s.d.; $n = 6$). Statistical differences are indicated by * ($p < 0.05$). Microscopic images at the bottom were obtained with an optical microscope after 12 days, demonstrating the extensive growth of L929 outside the 3D scaffold. This fact explains the high O.D. values reported for 2L929 and 3L929 at day 12.

and dimensions of the scaffolds: those of Osidak *et al.* are much more compact (higher infill) and width. According to the shape of our force-time curves (Figure 10A), all samples undergo reversible deformation throughout the strain range used, thus indicating that the 3D-bioprinted scaffolds behave like elastic solids (no yield point found during the experiment).

Cell-laden scaffolds (2L929 and 3L929) were able to maintain their hardness and elastic modulus (Figure 10) under culture conditions for up to 12 days. These results are particularly useful for *in vivo* implantation, since they imply that the bioprinted scaffolds can be subjected to *in vitro* maturation for 12 days prior to *in vivo* implantation without significant changes in their mechanical performance. On the other hand, the scaffolds without cells (2CTR and 3CTR) experienced a statistically significant reduction ($p < 0.05$) of both hardness (from 922.03 ± 22.15 g to 762.67 ± 105.9 g) and elastic modulus (from 0.48 ± 0.0219 kPa to 0.364 ± 0.0479 kPa) after 12 days under static *in vitro* culture conditions. As a possible hypothesis, the presence of cells could be producing some sort of structural framework (extracellular matrix sub-products) that minimizes and/or slows down loss of collagen mechanical properties[39-43]. The aforementioned hypothesis strengthens in keeping with other studies reporting that the higher is the cell-laden density, the lower are the mechanical properties of hydrogel-like scaffolds[44-46].

Despite the wide variability of compressive modulus values of collagen reported in the literature, the compressive hardness and elastic modulus values (Figure 10B and C) have the same order of magnitude as human brain tissue

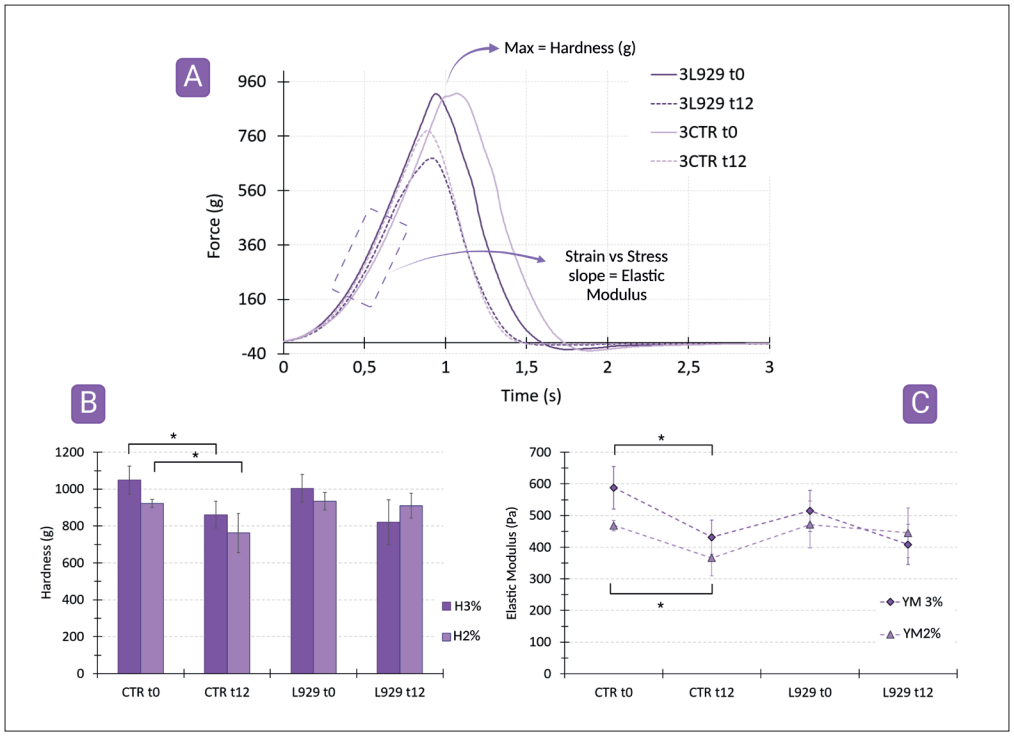

Figure 10. (A) Force vs time profile of 3CTR and 3L929 scaffolds. Profile of 2CTR and 2L929 scaffolds are identical. The maximum point belongs to 80% of strain deformation. Values of hardness (B) and compression Young's modulus (YM) or elastic modulus (C) obtained during the uniaxial compression test of 2CTR, 2L929, 3CTR, and 3L929 bioprinted scaffolds right after the bioprinting process and after 12 days. *$p < 0.05$ between samples.

or lungs[47-49]. Due to the complexity of native tissues and the differences with the artificially produced scaffolds (lower collagen concentration, low scaffold density; the CAD design is a grid instead of a solid mass), it is expected to obtain mechanical values that significantly differ from those of the collagen-rich tissues. The introduction of cells within the scaffold also requires concentration optimization to guarantee *in vitro* nutrients and oxygen diffusion. It is more realistic to compare the results with other bioprinted scaffolds made of type I collagen. The results reported herein are in agreement with those of xeno-free human skin-derived collagen biomaterial reported by Schmitt *et al.*[50] and with the collagen bioprinted scaffolds reported by Stepanovska *et al.*[51] in both cases working with type I collagen. It is well known that the mechanical performance of collagen bioinks rely on the composition, the collagen type and pore structure and that they can be improved by optimizing the crosslinking process or adjusting the collagen concentration[52]. Moreover, as previously mentioned, shape, dimensions and infill (compactness) of the scaffold subjected to compression can also alter the results. The influence of the collagen concentration in the mechanical performance can be observed in Figure 10B and C, where 3% (w/w) collagen (3CTR and 3L929) showed slightly higher hardness and elastic modulus than 2% (w/w) collagen scaffolds (2CTR and 2L929). We hypothesize that by just modifying the CAD design of the scaffolds, it would be possible to better adjust the mechanical properties. This hypothesis is supported by previous studies where the introduction of holes in the scaffolds significantly changes the compressive modulus[48].

Covalently crosslinked collagen possesses a stronger network with improved mechanical properties. Nevertheless, this can be detrimental to the scaffold permeability, which is crucial for cell viability, proliferation, migration, etc. The pH of the collagen-bioink is also of great importance not only for the cell viability but also for the mechanical performance of the construct. The study of Antoine *et al.* reported a clear dependence between the compression modulus and the pH value of collagen hydrogels[53]. The compressive modulus of 2CTR, 2L929, 3CTR, and 3L929 bioinks prepared with a final pH of 7.5–7.6 coincides with those reported by Antoine *et al.* for type I collagen hydrogels with the same pH. Finding a compromise between collagen mechanical properties, pH, and permeability is critical for 3D bioprinting and TE.

4. Conclusion

In this study, we investigated the suitability of two native, fibrous collagen masses (ColA and ColN) as 3D printing biomaterial inks and bioinks. Particularly, the collagen

neutralization, cell inclusion and 3D printing and bioprinting procedures were optimized and tested for reproducibility at different collagen concentrations, both for the acid and the neutral fibrillar collagen masses.

ColA has enough consistency for the production of complex scaffolds with a remarkable amount of layers (up to 27) without collapsing and maintaining superior shape fidelity. The acidic environment of this collagen mass makes it unsuitable for cell-laden bioinks, but the *in vitro* cytotoxicity studies demonstrated that it would be possible to print the mass and neutralize it post-printing, enabling cell seeding over the surface without jeopardizing cell viability. Nonetheless, the most attractive aspect of 3D bioprinting is the inclusion of cells in the bioink. Despite the remarkable performance of ColA in 3D printing, Viscofan S.A. has modified this collagen mass (ColN) to be easily neutralizable before the bioprinting process, making the inclusion of cells safer. This manuscript presents an adequate and effective protocol for ColN collagen neutralization by means of a biocompatible buffer (TRIS-HCl). The resulting neutral collagen mass was fully characterized and mixed with MSC-1 and L929 cells to produce scaffolds with proper printability and shape fidelity.

In light of the obtained results, it is possible to state that 3% (w/w) and 2% (w/w) of pure neutral collagen bioinks obtained from with ColN (without further ingredients) are suitable for the production of 3D scaffolds intended for tissue engineering. In fact, the pneumatic printing conditions (50–80 kPa) seem to have no significant effect on cell death, maintaining a cell viability over 90% even immediately right after the bioprinting process. Moreover, the printed scaffolds provided a stable platform for cell growth and proliferation in static culture conditions up to 2 weeks. Despite the promising results obtained, these biomaterial inks must be evaluated under the specific conditions of each particular application, especially when combined with other ingredients.

Acknowledgments

None.

Funding

This research was funded by Viscofan (S.A.) Centro para el Desarrollo Tecnológico Industrial (CDTI) IDI-20210050 and the Basque Country Government/Eusko Jaurlaritza (Department of Education, University and Research, Consolidated Groups IT907-16). Author Sandra Ruiz-Alonso thanks the Basque Country Government for the granted fellowship PRE_2021_2_0153. José M. Rey thanks the funding from the European's Union Horizon 2020 research and Innovation framework program (Triankle Project; Grant Agreement #952981). BioRender.com has been used as support for some figures assembly.

Conflict of interest

Authors Amaia Guembe, José M. Rey, Teresa Zúñiga, Jesús M. Izco and José I. Recalde declare that they work for the company Viscofan, while the rest declare no conflicts of interest.

Author contributions

Conceptualization: Jesús M. Izco, Jose Luis Pedraz, José I. Recalde

Data curation: Fatima Garcia-Villen, Amaia Guembe, José M. Rey, Teresa Zúñiga, Sandra Ruiz-Alonso

Formal analysis: Fatima Garcia-Villen, José M. Rey, Amaia Guembe, Teresa Zúñiga, Sandra Ruiz-Alonso

Funding acquisition: Jesús M. Izco, Jose Luis Pedraz

Investigation: Fatima Garcia-Villen, José M. Rey, Amaia Guembe, Teresa Zúñiga, Sandra Ruiz-Alonso

Methodology: Jesús M. Izco, Jose Luis Pedraz, José I. Recalde, Laura Saenz-del-Burgo, Fatima Garcia-Villen

Project administration: Jesús M. Izco, Jose Luis Pedraz

Resources: Laura Saenz-Del-Burgo, Jesús M. Izco, José I. Recalde, Jose Luis Pedraz

Supervision: Laura Saenz-Del-Burgo, Jesús M. Izco, José I. Recalde, Jose Luis Pedraz

Validation: Jesús M. Izco, Jose Luis Pedraz, José I. Recalde, Laura Saenz-Del-Burgo, Amaia Guembe, José M. Rey, Teresa Zuñiga

Writing – original draft: Fatima Garcia-Villen, Amaia Guembe, José M. Rey, Teresa Zuñiga, Sandra Ruiz-Alonso

Writing – review & editing: Laura Saenz-Del-Burgo, Jesús M. Izco, José I. Recalde, Jose Luis Pedraz

Ethics approval and consent to participate

Not applicable.

Consent for publication

Not applicable.

Availability of data

Authors elect not to share data.

References

1. Souza AG, Silva IBB, Campos-Fernandez E, *et al.*, 2018, Comparative assay of 2D and 3D cell culture models: Proliferation, gene expression and anticancer drug response. *Curr Pharm Des*, 24(15):1689–1694.

https://doi.org/10.2174/1381612824666180404152304

2. Zhang B, Gao L, Ma L, *et al.*, 2019, 3D bioprinting: A novel avenue for manufacturing tissues and organs. *Engineering*, 5(4):777–794.

   https://doi.org/10.1016/J.ENG.2019.03.009

3. Ng WL, Chua CK, Shen YF, 2019, Print me an organ! Why we are not there yet. *Prog Polym Sci*, 97(101145):1–45.

   https://doi.org/10.1016/J.PROGPOLYMSCI.2019.101145

4. Ashammakhi N, Ahadian S, Xu C, *et al.*, 2019, Bioinks and bioprinting technologies to make heterogeneous and biomimetic tissue constructs. *Mater Today Bio*, 1(100008):1–23.

   https://doi.org/10.1016/J.MTBIO.2019.100008

5. ASTM International, 2021, ISO/ASTM 52900:2021(E). Additive manufacturing—General Principles—Fundamentals and Vocabulary. ASTM International, Geneva, 1–5.

6. Zhuang P, Ng WL, An J, *et al.*, 2019, Layer-by-layer ultraviolet assisted extrusion-based (UAE) bioprinting of hydrogel constructs with high aspect ratio for soft tissue engineering applications. *PLoS One*, 14(6):e0216776.

   https://doi.org/10.1371/JOURNAL.PONE.0216776

7. Jiang T, Munguia-Lopez JG, Flores-Torres S, *et al.*, 2019, Extrusion bioprinting of soft materials: An emerging technique for biological model fabrication. *Appl Phys Rev*, 6(1):011310.

   https://doi.org/10.1063/1.5059393

8. Li X, Liu B, Pei B, *et al.*, 2020, Inkjet bioprinting of biomaterials. *Chem Rev*, 120(19):10793–10833.

   https://doi.org/10.1021/ACS.CHEMREV.0C00008/ASSET/IMAGES/LARGE/CR0C00008_0028.JPEG

9. Ng WL, Huang X, Shkolnikov V, *et al.*, 2022, Controlling droplet impact velocity and droplet volume: Key factors to achieving high cell viability in sub-nanoliter droplet-based bioprinting. *Int J Bioprinting*, 8(1):1–17.

   https://doi.org/10.18063/IJB.V8I1.424

10. Ng WL, Lee JM, Zhou M, *et al.*, 2020, Vat polymerization-based bioprinting—Process, materials, applications and regulatory challenges. *Biofabrication*, 12(2):022001.

    https://doi.org/10.1088/1758-5090/AB6034

11. Li W, Mille LS, Robledo JA, *et al.*, 2020, Recent advances in formulating and processing biomaterial inks for vat polymerization-based 3D printing. *Adv Healthc Mater*, 9(15):2000156.

    https://doi.org/10.1002/ADHM.202000156

12. Garcia-Villen F, Ruiz-Alonso S, Lafuente-Merchan M, *et al.*, 2021, Clay minerals as bioink ingredients for 3D printing and 3D bioprinting: Application in tissue engineering and regenerative medicine. *Pharmaceutics*, 13(1806):1–46 [Online]. Available:

    https://pubmed.ncbi.nlm.nih.gov/34834221/

13. Heid S, Boccaccini AR, 2020, Advancing bioinks for 3D bioprinting using reactive fillers: A review. *Acta Biomater*, 113:1–22.

    https://doi.org/10.1016/j.actbio.2020.06.040

14. Schwab A, Levato R, D'Este M, *et al.*, 2020, Printability and shape fidelity of bioinks in 3D bioprinting. *Chem Rev*, 120(19):11028–11055.

    https://doi.org/10.1021/acs.chemrev.0c00084

15. Groll J, Burdick JA, Cho DW, *et al.*, 2019, A definition of bioinks and their distinction from biomaterial inks. *Biofabrication*, 11(1):013001.

    https://doi.org/10.1088/1758-5090/aaec52

16. Postlethwaite AE, Seyer JM, Kang AH, 1978, Chemotactic attraction of human fibroblasts to type I, II, and III collagens and collagen-derived peptides. *Proc Natl Acad Sci U S A*, 75(2):871.

    https://doi.org/10.1073/PNAS.75.2.871

17. Min Lee J, Kang Qiang Suen S, Long Ng W, *et al.*, 2021, Bioprinting of collagen: Considerations, potentials, and applications. *Macromol Biosci*, 21(1):2000280.

    https://doi.org/10.1002/MABI.202000280

18. Marques CF, Diogo GS, Pina S, *et al.*, 2019, Collagen-based bioinks for hard tissue engineering applications: A comprehensive review. *J Mater Sci Mater Med*, 30(3):1–12.

    https://doi.org/10.1007/S10856-019-6234-X/TABLES/1

19. Damodaran S, Parkin KL, 2017, Philadelphia, Pennsylvania, United States. *Fennema's Food Chemistry*, 5th edn, CRC Press, Philadelphia, Pennsylvania, United States.

20. Schrieber R, Gareis H, 2007, Redhill, SURRE, United Kingdom. *Gelatine Handbook: Theory and Industrial Practice*, Wiley-VCH, Redhill, SURRE, United Kingdom.

21. Schmidt MM, Dornelles RCP, Mello RO, *et al.*, 2016, Collagen extraction process. *Int Food Res J*, 23(3):913–922. Accessed: July 14, 2022. [Online]. Available:

    https://www.cabdirect.org/cabdirect/abstract/20163160817

22. Suurs P, Barbut S, 2020, Collagen use for co-extruded sausage casings—A review. *Trends Food Sci Technol*, 102:91–101.

    https://doi.org/10.1016/J.TIFS.2020.06.011

23. Stepanovska J, Otahal M, Hanzalek K, *et al.*, 2021, pH modification of high-concentrated collagen bioinks as a factor affecting cell viability, mechanical properties, and printability. *Gels*, 7(4):252.

    https://doi.org/10.3390/GELS7040252

24. Osidak EO, Kozhukhov VI, Osidak MS, *et al.*, 2020, Collagen as bioink for bioprinting: A comprehensive review. *Int J Bioprinting*, 6(3):1–10.

    https://doi.org/10.18063/IJB.V6I3.270

25. Stuart K, Panitch A, 2008, Influence of chondroitin sulfate on collagen gel structure and mechanical properties at physiologically relevant levels. *Biopolymers*, 89(10):841–851.

    https://doi.org/10.1002/BIP.21024

26. Morozova S, Muthukumar M, 2018, Electrostatic effects in collagen fibril formation. *J Chem Phys*, 149(16):163333.

    https://doi.org/10.1063/1.5036526

27. Li Y, Qiao C, Shi L, *et al.*, 2014, Viscosity of collagen solutions: Influence of concentration, temperature, adsorption, and role of intermolecular interactions. *J Macromollecular Sci B*, 53(5):893–901.

    https://doi.org/10.1080/00222348.2013.852059

28. Osidak EO, Karalkin PA, Osidak MS, *et al.*, 2019, Viscoll collagen solution as a novel bioink for direct 3D bioprinting. *J Mater Sci Mater Med*, 30(3):1–12.

    https://doi.org/10.1007/S10856-019-6233-Y/FIGURES/6

29. Duan L, Li J, Li C, *et al.*, 2013, Effects of NaCl on the rheological behavior of collagen solution. *Korea-Australia Rheol J*, 25(3):137–144.

    https://doi.org/10.1007/S13367-013-0014-9

30. Newman S, Cloıp M, Allain C, *et al.*, 1997, Viscosity and elasticity during relevance to matrix-driven translocation. *Biopolymers*, 41:337–347.

    https://doi.org/10.1002/(SICI)1097-0282(199703)41:3

31. Shin YJ, Shafranek RT, Tsui JH, *et al.*, 2021, 3D bioprinting of mechanically tuned bioinks derived from cardiac decellularized extracellular matrix. *Acta Biomater*, 119:75–88.

    https://doi.org/10.1016/j.actbio.2020.11.006

32. Gao T, Gillispie GJ, Copus JS, *et al.*, 2018, Optimization of gelatin-alginate composite bioink printability using rheological parameters: A systematic approach. *Biofabrication*, 10(3):1–9.

    https://doi.org/10.1088/1758-5090/AACDC7

33. Lewis JL, Johnson SL, Oegema TR, 2004, Interfibrillar collagen bonding exists in matrix produced by chondrocytes in culture: Evidence by electron microscopy. *Tissue Engineering.*

    https://home.liebertpub.com/ten, 8(6):989–995.

    https://doi.org/10.1089/107632702320934083

34. Oechsle AM, Häupler M, Gibis M, *et al.*, 2015, Modulation of the rheological properties and microstructure of collagen by addition of co-gelling proteins. *Food Hydrocoll*, 49:118–126 [Online]. Available:

    https://www.sciencedirect.com/science/article/pii/S0268005X15001265

35. Boularaoui S, Al Hussein G, Khan KA, *et al.*, 2020, An overview of extrusion-based bioprinting with a focus on induced shear stress and its effect on cell viability. *Bioprinting*, 20:e00093.

    https://doi.org/10.1016/J.BPRINT.2020.E00093

36. Malekpour A, Chen X, 2022, Printability and cell viability in extrusion-based bioprinting from experimental, computational, and machine learning views. *J Funct Biomater*, 13(2):40.

    https://doi.org/10.3390/JFB13020040

37. Cunha JP, 2022, Tham (tromethamine injection).

    https://www.rxlist.com/tham-drug.htm (Accessed July 14, 2022).

38. Rhee S, Puetzer JL, Mason BN, *et al.*, 2016, 3D bioprinting of spatially heterogeneous collagen constructs for cartilage tissue engineering. *ACS Biomater Sci Eng*, 2(10):1800–1805.

    https://doi.org/10.1021/ACSBIOMATERIALS.6B00288/ASSET/IMAGES/LARGE/AB-2016-00288V_0007.JPEG

39. Diegelmann RF, Cohen IK, McCoy BJ, 1979, Growth kinetics and collagen synthesis of normal skin, normal scar and keloid fibroblasts in vitro. *J Cell Physiol*, 98(2):341–346.

    https://doi.org/10.1002/JCP.1040980210

40. Ueno H, Nakamura F, Murakami M, *et al.*, 2001, Evaluation effects of chitosan for the extracellular matrix production by fibroblasts and the growth factors production by macrophages. *Biomaterials*, 22(15):2125–2130.

    https://doi.org/10.1016/S0142-9612(00)00401-4

41. Freundlich B, Bomalaski JS, Neilson E, *et al.*, 1986, Regulation of fibroblast proliferation and collagen synthesis by cytokines. *Immunol Today*, 7(10):303–307.

    https://doi.org/10.1016/0167-5699(86)90067-8

42. Goldberg B, Green H, 1964, An analysis of collagen secretion by established mouse fibroblast lines. *J Cell Biol*, 22:227–258. Accessed: May 19, 2022. [Online]. Available:

    http://rupress.org/jcb/article-pdf/22/1/227/1401992/227.pdf

43. Kosir MA, Quinn CCV, Wang W, *et al.*, 2000, Matrix glycosaminoglycans in the growth phase of fibroblasts: More of the story in wound healing. *J Surg Res*, 92(1):45–52.

    https://doi.org/10.1006/JSRE.2000.5840

44. Gold KA, Saha B, Rajeeva Pandian, NL, *et al.*, 2021, 3D bioprinted multicellular vascular models. *Adv Healthc Mater*, 2101141:1–14.

    https://doi.org/10.1002/adhm.202101141

45. Tian X, Chen X, 2014, Effects of cell density on mechanical properties of alginate hydrogel tissue scaffolds. *J Biomimetics Biomater Tissue Eng*, 19:77–85.

    https://doi.org/10.4028/WWW.SCIENTIFIC.NET/JBBTE.19.77

46. Buckley CT, Thorpe SD, O'Brien FJ, *et al.*, 2009, The effect of concentration, thermal history and cell seeding density

on the initial mechanical properties of agarose hydrogels. *J Mech Behav Biomed Mater*, 2(5):512–521.

https://doi.org/10.1016/J.JMBBM.2008.12.007

47. Singh G, Chanda A, 2021, Mechanical properties of whole-body soft human tissues: A review. *Biomed Mater*, 16(6):062004.

https://doi.org/10.1088/1748-605X/AC2B7A

48. Tang-Schomer MD, White JD, Tien LW, *et al.*, 2014, Bioengineered functional brain-like cortical tissue. *Proc Natl Acad Sci U S A*, 111(38):13811–13816.

https://doi.org/10.1073/PNAS.1324214111/-/DCSUPPLEMENTAL/PNAS.201324214SI.PDF

49. Engler AJ, Sen S, Sweeney HL, *et al.*, 2006, Matrix elasticity directs stem cell lineage specification. *Cell*, 126(4):677–689.

https://doi.org/10.1016/j.cell.2006.06.044

50. Schmitt T, Kajave N, Cai HH, *et al.*, 2021, In vitro characterization of xeno-free clinically relevant human collagen and its applicability in cell-laden 3D bioprinting. *J Biomater Appl*, 35(8):912–923.

https://doi.org/10.1177/0885328220959162

51. Stepanovska J, Supova M, Hanzalek K, *et al.*, 2021, Collagen bioinks for bioprinting: A systematic review of hydrogel properties, bioprinting parameters, protocols, and bioprinted structure characteristics. *Biomedicines*, 9(9):1–30.

https://doi.org/10.3390/BIOMEDICINES9091137

52. Chen C, Zhao ML, Zhang RK, *et al.*, 2017, Collagen/heparin sulfate scaffolds fabricated by a 3D bioprinter improved mechanical properties and neurological function after spinal cord injury in rats. *J Biomed Mater Res A*, 105(5):1324–1332.

https://doi.org/10.1002/JBM.A.36011

53. Antoine EE, Vlachos PP, Rylander MN, 2015, Tunable collagen I hydrogels for engineered physiological tissue micro-environments. *PLoS One*, 10(3):e0122500.

https://doi.org/10.1371/JOURNAL.PONE.0122500